Real-Time Control of Selective Laser Melting for Fabrication of Miniaturized Structures

L. Wasmer[1], D. Seiler[1], J. Hänggi[1], G. Ragonese[2], M. de Wild[1]

[1] *University of Applied Sciences Northwestern Switzerland, FHNW, School of Life Sciences HLS, Institute for Medical Engineering and Medical Informatics IM², Muttenz, CH*

[2] *Politecnico di Torino, Department of Mechanical and Aerospace Engineering, Torina, IT*

INTRODUCTION: The miniaturization of additive manufacturing technologies like Micro-Selective Laser Melting (µSLM) enables the production of increasingly smaller structures with exceptional precision. However, the exact control of the laser melting process within the powder bed plays a critical role.[1] Maintaining a consistent laser power is essential to avoid inhomogeneous heat distribution across different geometric regions within the component. Inadequate control like local overheating can result in undesirable outcomes such as geometric deformities, porosity, warping, distortion, agglomeration, and surface irregularities and compromises the creation of fine structures.

METHODS: By utilizing high-speed pyrometer, optimal target temperatures for the melt pool can be identified. In state-of-the-art µSLM systems, laser power can then be dynamically regulated through a pyrometer-based real-time feedback loop, ensuring precise control of the laser power over various time scales. We demonstrate the application of a µSLM system (ø55 mm platform diameter, 400 W single-mode cw fiber laser, spot size 40 µm, AconityMINI, Aachen, Germany) equipped with dual pyrometry for monitoring the thermal radiation emitted by the melt pool in CoCr powder (d_{50} = 13.5µm, Nanoval, Berlin, Germany).

RESULTS: Fig. 1 shows the positive influence of the pyrometer-controlled feedback.

DISCUSSION & CONCLUSIONS*:* Our research showcases that the implementation of real-time control mechanisms in the manufacturing process using µSLM technology leads to the production of finer CoCr structures, improved overhangs, smoother surfaces, and denser microstructures. This highlights the potential of in-process control strategies in enhancing the quality and efficiency of additive manufacturing processes. This advancement presents novel opportunities, particularly in the realm of medical applications. However, the establishment of the material-dependent set value and PID parameters for real-time control of the pyrometer target value is a prerequisite.

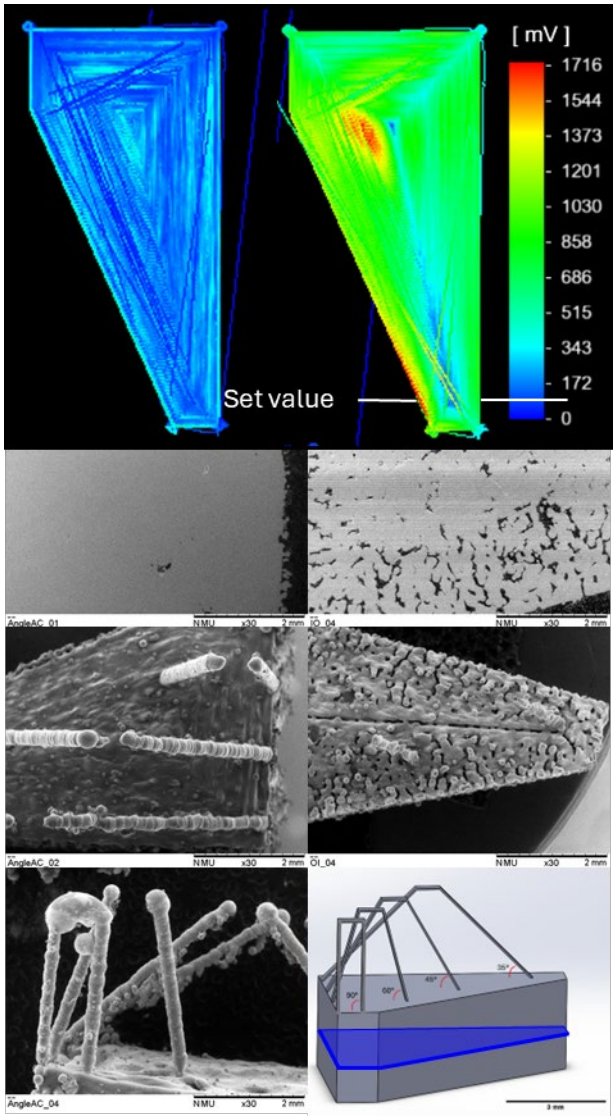

Fig. 1: Comparing µSLM with (left) and without (right) pyrometric feedback:
1st row: Spatially resolved pyrometric mapping of heat emission. 2nd: SEM of cross section through solid part (1%, resp. 20% porosity).
3rd/4th: SEM and CAD model of ø220 µm struts with 35°, 45°, 60° and 90° inclination.

REFERENCES: [1] T. Al-Saadi et al., *In-situ process control strategies for selective laser melting*, IFAC-PapersOnLine, 56, 2, 2023, 6594-6599.doi.org/10.1016/j.ifacol.2023.10.357

Advanced selective titanium anodization of machine-readable codes

Ali Mohamad Mahmoud[1], Pierre-Antoine Gay[1], Camille Cardot[2], Amandine Fluchot[2], Joël Matthey[1,2]

[1] University of Applied Sciences Haute Ecole Arc Ingénierie CH,
[2] Positive Coating SA, CH

INTRODUCTION: The Unique Device Identification (UDI) is a distinctive numeric or alpha-numeric code related to a medical device or an implant. It consists of a clear and unambiguous identification of specific devices on the market, and it facilitates their traceability throughout their entire life cycle. One approach to generate such codes is laser marking the surface.

METHODS: The interaction of a laser beam with titanium alloys can locally modify the surface properties, namely it can weaken the corrosion resistance of the textured zone. To reinforce the surface properties, a selective titanium anodization process has been developed by means of the Atomic Layer Deposition (ALD). ALD is known to produce pinhole-free and conformal oxide thin films. Sarting with either bare or pre-treated titanium, an amorphous alumina thin film of 160 nm is grown by ALD at 150°C. The precursors used to form the Al_2O_3 coating are trimethylaluminum and water vapor. The aim is to electrically insulate the surface. Then, laser marking is performed with a femtosecond laser system to remove locally the dielectric coating and, simultaneously, smoothly engrave the surface (depth few microns). The outcome is the formation of a current divider at the surface due to freshly ablated titanium and the dielectric properties of the remaining alumina. By applying a controlled voltage, the next step is to anodize selectively the laser-textured code in a sulfuric acid solution (2% vol.), stabilized at 20°C. The final step consists of dissolving the amorphous alumina in an ultrasonic alkaline solution (pH 12.5). Even though titanium alloy properties have been modified by the laser beam, the converted oxide offers an extra protection against corrosion.

RESULTS: The feasibility of a corrosion-resistant 1.5 mm x 1.5 mm machine-readable code has been demonstrated. Not only the performances are increased but also the colored UDI can be used as a marketing vehicle.

Fig. 1: UDI code obtained with the selective the titanium anodization process

DISCUSSION & CONCLUSIONS: By combining chemical vapor deposition, laser and electrochemical technologies, a selective titanium anodization process has been developed. The innovation relies on the substitution of standard lacquer masking methods by an ultrathin amorphous alumina coating. The benefit of the sacrificial ALD masking can be found in the fact that it allows the production of loose parts. Additionally, the mask stripping process does not require any solvent. Finally, the process can be easily scaled up to the industry.

ACKNOWLEDGEMENTS: The authors thank ZimVie company for providing the samples.

Towards Biocompatible Immobilized Antibacterial Coatings on Titanium which kill bacteria on contact

J.J.T.M Swartjes, T. Loontjes, R. Li, Y. Sheng

[1]*Bioprex Medical, Blauwborgje 31, 9747 AC, Groningen, the Netherlands*

INTRODUCTION: Antibiotic resistance is one of the largest threats towards global health. Infections are the number one cause of implant failure and with an aging population and improving healthcare in developing countries, its costs and consequences are expected to rise dramatically. Preventing infection by antibacterial coatings is an attractive alternative compared to treatment only. Here, we present an immobilized contact-killing coating, based on a Quaternary Ammonium Compound, successful in preventing bacterial adhesion and subsequent infection.

METHODS: Titanium surgical plates (10 x 4 x 1 mm) were dip coated using a solution of 10% (w/w) hyperbranched polymer, followed by a solution of 25% (w/w) polyethyleneimine. Both steps were followed by curing at elevated temperature for several hours. Quaternization was achieved by addition of 10 mM NaI. Antibacterial activity was tested using the Japanese Industry Standard (JIS) test, using several clinically relevant bacterial strains.

RESULTS: Bacterial strains were tested for their adhesion on coated titanium and reduction ranged from 90 to 100%. SEM images confirmed killing of bacteria by contact, as indicated by the disruption of the cell structure and the release of internal proteins and other substances. An *in-vivo* murine infection model confirmed the ability to prevent infection *in-situ* and showed good biocompatibility.

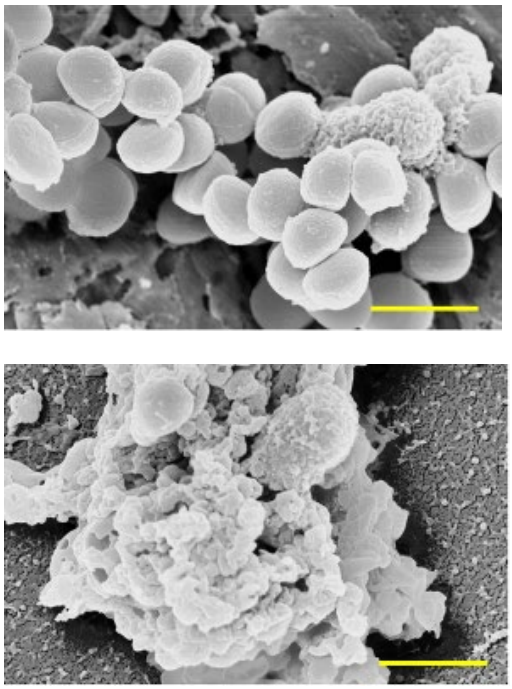

Figure 1. *SEM images of bacteria on untreated titanium (top) and titanium coated with HBP-PEI followed by quaternization with NaI (bottom). Scale bars represent 1µm.*

DISCUSSION & CONCLUSIONS: Implant associated infection are notoriously hard to eradicate due to the resistant nature of biofilms. Prevention by conventional methods such as antibiotics is suffering from antimicrobial resistance and alternatives are scarce. Here, we present a QAC capable of killing bacteria upon contact with the surface, preventing their formation of biofilms. The polyurea coating is durable, withstanding forces commonly seen during placement of (orthopaedic) implants and since its working mechanism is not based on release, it is not depleted during use, offering prolonged protection.
Preliminary *in-vivo* results show good biocompatibility as well as reduction of bacterial challenge for up to at least 4 days, the complete study duration.

Towards an accurate prediction of magnesium biocorrosion by closer mimicking the in-vivo environment

M. Yalcinkaya, A. Bruinink, M. Cihova, P. Schmutz

Laboratory for Joining Technologies and Corrosion, Empa - Swiss Federal Laboratories for Materials Science and Technology, Dübendorf CH-8600, Switzerland

INTRODUCTION: Magnesium (Mg) has attracted great interest as a biodegradable metallic implant due to the formation of bioresorbable corrosion products during its degradation in the body. Yet, a challenge in the reliable prediction of degradation mechanism is that currently performed in-vitro experiments typically induce the formation of corrosion products with different chemical structures and transport properties than those observed in animal studies (in-vivo) [1].

From a materials perspective, another complexity level is generated by the low solubility of alloying and impurity elements in magnesium, resulting in the formation of cathodic secondary intermetallic phases (IMP's) [2]. As the majority of published in-vitro studies involved such heterogeneous Mg surfaces, it remains unclear, if the corrosion product layer actually limits magnesium's anodic oxidation or decreases the cathodic reactivity of secondary phases.

To investigate the influence of these cathodic secondary phases on the Mg corrosion behavior in a physiological mimicking environment, an experimental setup was developed to include often overlooked in-vivo aspects such as solution flow, physiological pH buffering on Mg surface. Two very different materials were compared: low-purity Mg (99.9 wt% Mg; Fe >200 ppm), which contains a high amount of Fe-rich intermetallic phases, and ultra-high purity magnesium (XHP) (>99.999 wt% Mg; Fe <1 ppm) as a homogenous substrate without any secondary phase.

METHODS: Samples were exposed to our new formulation, based on an extensive literature review of the real measured values of inorganic ions and organic species, of a simulated interstitial body fluid (SIBF) that mimics the composition of human interstitial body fluid [3]. The pH of SIBF is regulated with dynamic bicarbonate buffering and flown over Mg. The electrochemical reactivity of Mg samples was then evaluated by performing Electrochemical Impedance Spectroscopy (EIS). The samples were subsequently characterized using Scanning Electron Microscopy/Energy Dispersive X-ray Spectroscopy (SEM/EDS).

RESULTS: Fig.1 shows that the precipitation of corrosion products forms a micrometer-thick porous intermediate layer allowing but limiting ionic/water transport on the Mg matrix and IMP's.

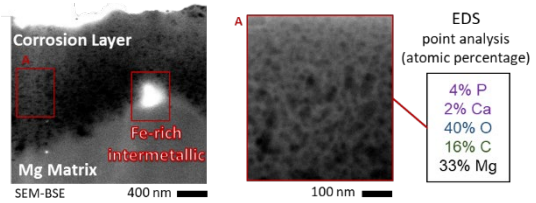

Fig. 1: Ion-milled cross-section of low-purity Mg, after 24 in SIBF (37 °C, 1 µl/sec, pH 7.4)

The EIS results further indicated dramatically reduced cathodic reactivity of IMP's, where the obtained values became comparable to the one obtained for ultra-high purity Mg.

To reveal the individual effect of precipitations, ion-specific products properties were studied for both purity degrees. This approach made it possible to isolate and assess the barrier effect of Mg-hydroxide, Mg-phosphate, and Ca-phosphate on a heterogonous and homogenous surface.

DISCUSSION & CONCLUSIONS: Free Ca^{2+}, Mg^{2+} and PO_4^{3-} ions levels can cause opposite effects on corrosion mechanisms depending on the presence of Fe-rich intermetallic phases. Therefore, observed microstructure-dependent variations between in-vivo and in-vitro studies may be mainly caused by non-physiological test solutions and pH buffering. We further aim to understand how organic compounds and pH levels affect corrosion products to provide a more nuanced understanding of Mg biocorrosion.

REFERENCES: [1] J. Walker, S. Shadanbaz, N. Kirkland, et al (2012) *J Biomed Mater Res B Appl Biomater* **100**:1134-41. [2] D. Höche, C. Blawert, S. V. Lamaka, et al (2016) *Phys. Chem. Chem. Phys.* **18**:1279-91. [3] A. Bruinink, *Handbook of Biomaterials* RSC (in press)

ACKNOWLEDGEMENTS: The authors would like to acknowledge the Metrohm Foundation for the financial support of this research.

Influence of different potentials during electropolishing on the corrosion behaviour of a magnesium alloy

J. Kloiber[1,2], U. Schultheiß[1,3], V. Anetsberger[1], H. Hornberger[1,2,3]

[1]*Biomaterials Laboratory, Faculty of Mechanical Engineering, Ostbayerische Technische Hochschule (OTH) Regensburg, Seybothstraße 2, 93053 Regensburg, Germany,*

[2] *Regensburg Center of Biomedical Engineering (RCBE), Ostbayerische Technische Hochschule (OTH) Regensburg, Seybothstraße 2, 93053 Regensburg, Germany,*

[3] *Analytics Center, Faculty of Mechanical Engineering, Ostbayerische Technische Hochschule (OTH) Regensburg, Seybothstraße 2, 93053 Regensburg, Germany*

INTRODUCTION: Electropolishing is an attractive surface treatment to improve the corrosion behaviour of magnesium for temporary implant applications [1], but it is not well known how different polishing potentials affect the degradation of this bioresorbable metal.
The aim of this study was to investigate the influence of a potential variation during electropolishing on the corrosion behaviour of AZ31.

METHODS: Electropolishing of the AZ31 samples was carried out in a mixture of phosphoric acid, ethanol and deionized water at different potentials from the Open Circuit Potential (OCP) to the transpassive region (vs. Ag/AgCl 3M) (Fig. 1, left).
The degradation behaviour was observed by potentiodynamic polarization in Dulbecco´s Modified Eagle´s Medium (DMEM) (Fig. 1, right).

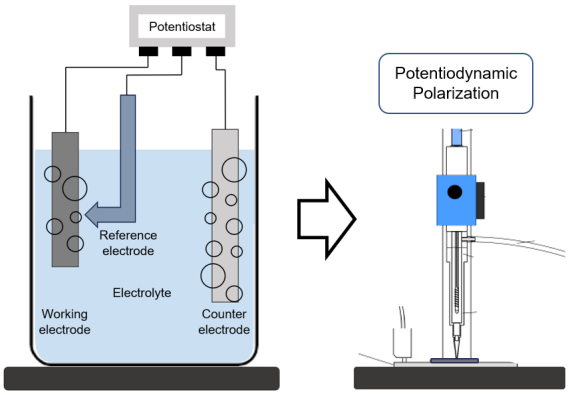

Fig. 1: Schematic illustration of the electropolishing setup (left) and the in vitro testing of the degradation behaviour of electropolished AZ31(right).

RESULTS: The developed electropolishing process improved the magnesium surface by providing a bright and mirror-like surface, a low roughness and a low corrosion rate. Electropolishing reduced the corrosion rate to 0.1 mm/year (at 200 mV) compared to 1.28 mm/year after mechanical grinding (MGrid) (Fig. 2).

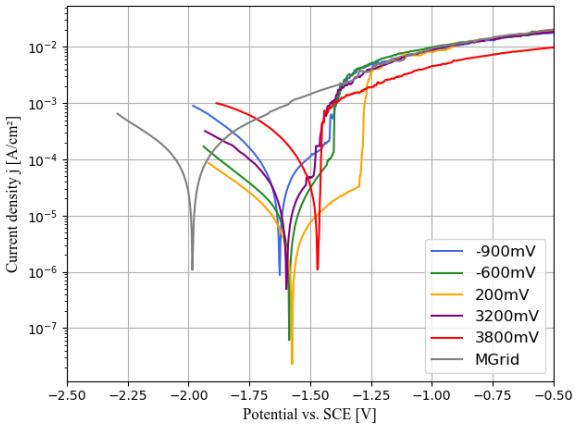

Fig. 2: Corrosion behaviour of a mechanically ground magnesium alloy AZ31 compared to the electrochemically treated samples electropolished at five different potentials.

DISCUSSION & CONCLUSIONS: In principle, potentials in the passive and transient range not only lead to a reduction in roughness, but also to a significant increase in corrosion stability. To assess the long-term corrosion behaviour, future investigations of the surface layer formed after electropolishing must be carried out.

ACKNOWLEDGEMENTS: We gratefully thank Regensburg Center of Biomedical Engineering (RCBE) for the support of laboratory consumables.

REFERENCES: [1] J. Kloiber et al. (2023) Mater. Today Commun. 38:107983.

MONITORING THE TECHNICAL CLEANLINESS OF IMPLANTS USING CORRELATIVE MICROSCOPY

M. Hiltl[1], C. Gohil[1], H. Brandenberger[2]

[1]*Carl Zeiss Industrial Quality & Research, Oberkochen, D,*

[2] *Gloor Instruments AG, Kloten, CH*

INTRODUCTION: Medical products, such as implants, have a direct impact on peoples' lives, and producing a contaminated product would pose a high health risk to the patient. To avoid such cases, medical technology companies need to fulfill stringent regulatory requirements stipulated by various authorities regarding quality. For this reason, technical cleanliness plays a key role in quality assurance, within all aspects of the medical industry, e.g., manufacturing, production, production environment, packaging and even transportation. Solutions are ready for deployment at every step of the process to detect and characterize particulates that should not be present; a mandatory requirement when looking to comply with regulations, whilst improving productivity through reduced scrap and/or rework.

METHODS: The analysis of residual dirt or particulate contaminants arising during an individual production process can (in addition to light microscopy) also be determined by automated particle analysis using a Scanning Electron Microscope (SEM). The SEM allows a high spatial resolution down to nanoscale, a high depth of field and combined with Energy Dispersive X-ray Spectroscopy (EDS) provides vital elemental composition of each particulate contaminant. Light and electron microscopes are complemented by the correlative solution approach (correlative microscopy) which is also open to other analytical methods. The correlative workflow allows quick and easy relocation of regions of interests, across different imaging methods and analysis technologies. The coordinates of a critical particulate contaminant or a critical area can easily be transferred between each system and thus allowing to use various visual and analytical methods, all from the exact same location.

RESULTS: This supplementary multi-modal data from the various correlative methods, provides more answers to the key questions of where, why, and how many contaminates are being detected. This approach allows to take preventive steps, which eliminates contamination, ensures high quality standards, optimum functionality and longevity of the medical implants being produced.

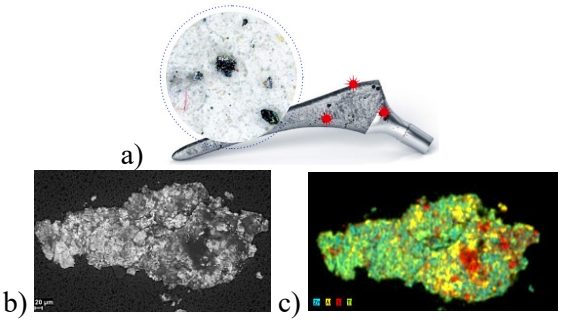

Fig. 1: Contaminated implant: Correlative particle analysis using a) light and b) electron microscope with c) EDS elemental mapping. Ti [green], Si [red], Al [yellow], Zn [blue].

DISCUSSION & CONCLUSIONS: Medical manufacturers, suppliers and end users demand ever-increasing quality standards, so advanced technical cleanliness is fundamental to eradicating contamination from manufactured parts and components, including the relevant quality gates along the entire production chain. The automated workflow and the correlative microscopy approach are a step forward in detecting and classifying particulate contamination, and facilitating to comply with industry quality standards, including GxP regulations. The GxP good practice makes the analyzes steps traceable and therefore compliant with regulations and certification requirements (e.g., VDI 2083 Part 21).

SUB-MICRON X-RAY CT ACCURACY THANKS TO METROLOGICAL SCAN TRAJECTORY

S. Burkhard[1], A. Küng[1]

[1]*Federal Institute of Metrology METAS, Bern-Wabern, Switzerland*

INTRODUCTION: Real case studies are presented of a unique X-ray computed tomography (CT) system for technical applications which is capable of reaching sub-micron accuracy for small objects (< 4 mm) with dimensional traceability, providing exceptional measurement capabilities for complex-shaped objects.
This level of accuracy is made possible by precisely measuring the full CT system geometry for every projection during a scan and incorporating this geometrical information in the reconstruction of the scan volume, combined with highly stable environmental conditions. In addition to correcting unwanted movements of the setup during a scan, this metrological setup can also be used for extending conventional circular scans to flexible trajectories, improving image sharpness uniformity throughout the scan volume.

METHODS: The metrological measurement of the CT system geometry relies on 3 different methods (Fig. 1):
1. The positions of the rotation axis and detector stages along the X-ray beam axis and the vertical position of the sample are measured using calibrated infrared laser interferometers
2. Mechanical movements of the X-ray tube and transverse movements of the rotation axis and detector stages are tracked using laser beams in the visible range directed at CMOS sensors
3. Movements of the X-ray focal spot relative to the X-ray tube are detected by analysing the projected positions of markers mechanically mounted on the X-ray tube in the radiographies.

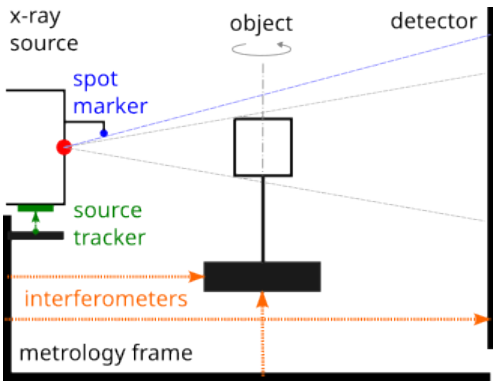

Fig. 1: Schematic of the metrological CT setup

The projective magnification of the System is calibrated using a traceably characterized reference object. The interferometric measurement of changes in the rotation axis and detector stages preservers traceability of the system unless an interferometer beam is disrupted.

RESULTS: While the general accuracy of this system has previously been demonstrated for sphere centre distances [1], which have limited sensitivity to image blurring and surface determination offsets, the incorporation of all geometrical information and focal spot movements in particular for the volume reconstruction can lead to a significant improvement of local image sharpness (Fig. 2).

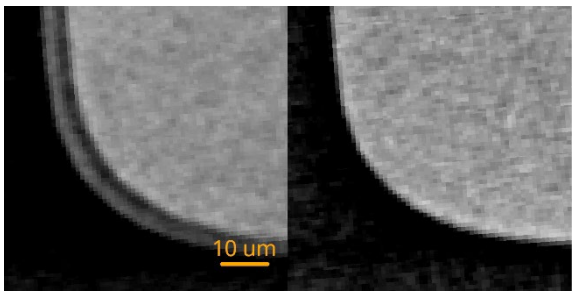

Fig. 2: Example of local image sharpness of conventional circular reconstruction (left) vs. metrological reconstruction (right) of the same data of a steel object at a voxel size of 0.9 µm.

DISCUSSION & CONCLUSIONS: Such an X-ray CT system is capable of reliably producing traceable dimensional measurements with sub-µm accuracy for small objects (< 4 mm for 1 µm voxel size). Measurements of hole diameters with < 1 µm accuracy (relative to tactile reference measurements) have even been achieved in 8 mm steel samples with 2.15 µm voxel size.

REFERENCES:

[1] Bircher BA, Meli F, Küng A, Thalmann R (2020) METAS-CT: metrological X-ray computed tomography at sub-micrometre precision. The 20th EUSPEN International Conference, 281–284.

Grain size measurement of ceramic materials using deep learning

S. Jakobs[1]

[1]*RMS Foundation, Bettlach, Switzerland*

INTRODUCTION: Grain size determination is crucial for characterizing materials, particularly ceramics, as their microstructure impacts properties and performance of the material. Traditional manual methods like line-intercept counting are labour-intensive and prone to human error. According to [1], manual determination of grain size will deviate by ±10% from the true grain size, depending on the number of grains evaluated, the number of phases and the homogeneity of the material.
Machine learning, particularly neural networks like U-Net [2], offer a more efficient and consistent approach, processing large datasets. This study applies a U-Net Algorithm to SEM images of Al_2O_3 & ZrO_3 ceramic material, demonstrating its effectiveness in grain boundary segmentation.

METHODS: The dataset consisted of 30 raw images, each 2048×1536 pixels in resolution. 15 images were randomly chosen and split into 90% training and 10% test sets. The remaining 15 images were used for validation of the process at the end. In the first 15 images, the grain boundaries were labelled red by hand and the image was then converted to a binary image so that only the grain boundaries remained (see Fig. 1). Once the image with the binary grain boundaries is available, the grain sizes can be analysed using classical methods (e.g. watershed algorithm). For the input into the neural network, all images were divided into 512×512 patches, and data augmentation (rotation and mirroring) increased the dataset eightfold, resulting in 96 patches per image. The U-Net model, widely used for image segmentation, was structured with five layers and contained 1.9 million parameters. The model's performance was assessed using IoU (Intersection over Union) and Dice scores, with comparisons made against manually measured grain sizes following ISO standards [1].

RESULTS: For the evaluation of the procedure, the 15 validation holdback images underwent manual analysis, and the results were compared. The average deviation from manual analysis was 4.5%. The determination of the grain size was separated by phase using histogram thresholding of the grey values of the images (see Fig. 2).

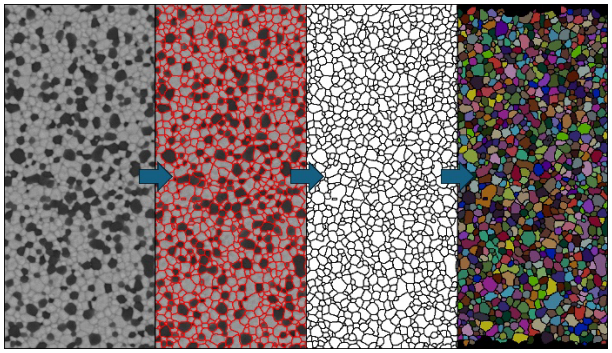

Fig. 1: Once the neural network has been trained, the labour-intensive labelling step can be done by the algorithm.

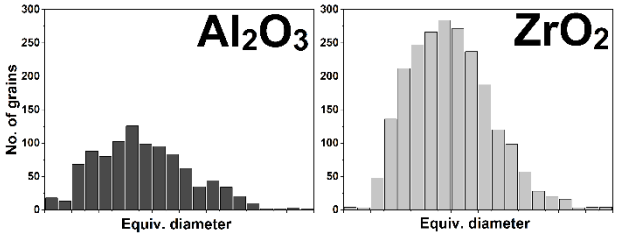

Fig. 2: Result of the segmentation of Fig. 1, with differentiation by phase.

DISCUSSION & CONCLUSIONS: This study emphasises the effectiveness of neural networks for automatic grain size measurement in SEM images of ceramic materials. The neural network provides a consistent assessment, reduces subjective bias and offers a reliable alternative to manual segmentation. In addition, more data can be obtained in less time. New characteristics of the grains, such as aspect ratio or orientation, could also be analysed without additional effort. Histograms, as shown in Figure 2, are also very difficult to produce manually. Visual evaluation remains important, as IoU and Dice scores do not always align with visual impressions.

ACKNOWLEDGEMENTS: This project was internally funded by RMS Foundation.

REFERENCES:

[1] ISO 13383-1:2016
[2] O. Ronneberger et al., "U-Net: Convolutional Networks for Biomedical Image Segmentation," MICCAI, vol. 9351, pp. 234-241, 2015).

THE IDENTITY OF IMPLANT MATERIALS GOVERNS THE ANTIMICROBIAL EFFICACY OF SET-M33

A. Maranesi[1,4], S. Mohammadi[2], I. Castañon [3], C. Falciani [3], W. Unger [2*], A. Ferrari [4*]

[1]Universitat Politècnica de Catalunya, Department of Material Science and Engineering, Barcelona, Spain, [2]Erasmus University Medical Centre, Department of Pediatrics, Rotterdam, Netherlands, [3]Dipartimento di Biotecnologie Mediche, Universita` degli Studi di Siena, Siena, Italy, [4]Hylomorph AG, Technopark, Zurich, Switzerland

INTRODUCTION: CIED implant infections are challenging due to their recurrence and resistance to standard antibiotics, despite antiseptic protocols. Opportunistic pathogens like Staphylococci and E. coli are common[1]. Antimicrobial peptides (AMPs) such as SET-M33 offer a solution by targeting bacterial membranes without fostering resistance[2]. This study explores SET-M33's efficacy when used with CIED implant materials (titanium, silicone, PTFE) and protective envelope materials (Biocellulose, PLGA electrospun membrane, and PGA mesh).

METHODS: Material surface properties (roughness, hydrophilicity, porosity) were assessed. SET-M33 was synthesized via Fmoc chemistry, functionalized with TAMRA, and tested for diffusion through protective envelopes. Materials soaked in SET-M33 were inoculated with E. coli and S. aureus and incubated overnight. Antimicrobial efficacy was evaluated by colony counting.

RESULTS: The tested materials displayed distinct surface characteristics, with porosity being a critical factor in the diffusion of SET-M33 through the envelope materials, with PGA mesh having the highest porosity and BC the lowest. BC retained 56% of the peptide, reducing its efficacy, while PGA allowed complete release in 90 minutes.

SET-M33 combined with envelope materials showed enhanced antibacterial activity compared to direct coating on titanium and silicon, with BC achieving full bacterial inhibition. However, low-porosity materials limited diffusion, restricting the effect to treated sides**.**

Table 1. Diffusion rates and effective diffusion coefficients of TAMRA-SETM33 across three types of membranes: BC, Espn, and Mesh

Envelope materials	Diffusion rate (mg/h)	D_{eff} (cm²/h)	Drug loss (%)
BC	$0.7\times10^{-3} \pm 5.9\times10^{-5}$	0.0083 ± 0.0005	56.3 ± 1.7
Espn	$1.4\times10^{-3} \pm 5\times10^{-5}$	0.003 ± 0.001	14.3 ± 1.7
Mesh	$4.126\times10^{-1} \pm 0.007$	1.07 ± 0.11	0

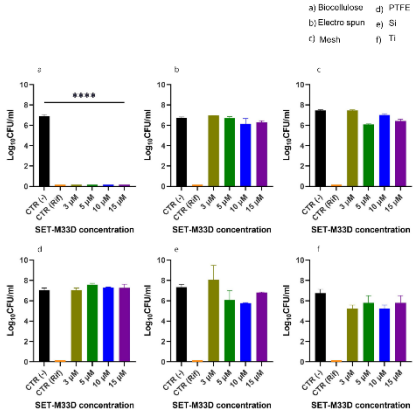

Fig 1. Quantitative growth of S. aureus on BC (a), Espn (b), Mesh (c), PTFE (d), Si (e) and Ti (f) treated with increasing concentrations of SET-M33D, compared to untreated and Rifampin treated controls.

DISCUSSION & CONCLUSIONS: SET-M33 has potential as an antimicrobial agent for protecting CIED implants, either through direct coating on implant materials or in combination with protective envelope materials. However, its current formulation is less effective when applied as a simple coating on implant surfaces. The efficacy of SET-M33 improves when used with envelope materials, which can better absorb the peptide solution. Nonetheless, low-porosity membranes limit diffusion, leading to partial antimicrobial protection. Future research will focus on optimizing the peptide structure to reduce steric hindrance or improve interactions with surfaces of varying roughness and hydrophilicity, enhancing its protective capability

ACKNOWLEDGEMENTS: This work was supported by a European Union Horizon Europe MSCA DN-ID grant (grant number 101073263)

REFERENCES:

1. Gutiérrez-Carretero,E.*et al.*. *Microorganisms* 12, (2024).
2. Cresti, L. *et al.*. *Pharmaceutics* 15, (2023)